Outer-core emission spectra of heavy alkali metals

R. L. Fink,* P. N. First,† and C. P. Flynn
Department of Physics, 1110 West Green Street, University of Illinois at Urbana-Champaign, Urbana, Illinois 61801
(Received 8 February 1988)

We report $np^5(n+1)s^2 \rightarrow np^6(n+1)s$ emission spectra of K ($n=3$), Rb ($n=4$), and Cs ($n=5$), and compare emission-band characteristics through the series Na–Cs using earlier data for Na. The normalized band profiles of the different alkali metals are remarkably similar when scaled by the Fermi energy E_F. However, the spin-orbit partner intensity ratios are far from the ideal value 2, reaching approximately 60 for Rb and above 65 for Cs, mainly owing to Coster-Kronig decays from higher levels. We confirm that the Mahan–Nozières–De Dominicis "anomaly" at E_F is generally weaker in emission than in absorption. It decreases through the series to become undetectable for emission from Cs. A systematic increase of the core-hole-lifetime width occurs through the column of alkali metals from a reported estimate of 10 meV for Na to a value of 50 meV for Cs. A study of the Fermi-edge shape between 20 and 300 K reveals temperature-dependent phonon broadening in generally good agreement with theoretical predictions. Incomplete relaxation plays only a minor role in the edge processes of the heavy alkali metals. Additional Fermi-edge broadening and the shifted emission edges of surface atoms are observed for alkali-metal films 10–100 Å thick.

I. INTRODUCTION

Much research into core spectroscopy is directed towards a detailed understanding of the solid-state factors that influence the core-excitation line shapes of solids.[1] In addition to mechanisms present also in nonmetals, core line shapes of metals reveal that the band excitations begin abruptly from zero energy. Their emission bands therefore exhibit a sharp cutoff at the Fermi energy, E_F, and Auger processes with band excitations open fast channels for core-hole decay, as first described by Skinner.[2] Other more subtle effects of the conduction-electron liquid on core spectra are visible also. Many of these phenomena are now understood in general terms, and semiquantitative theories are available to describe them.[1] There remains a lack of accurate measurements carried through systematically on chosen systems. Definitive comparisons between theory and experiment are therefore rare. The present work was undertaken with these needs in mind.

Alkali metals provide useful tests for fundamental theories of core processes. Here we focus on the series of $np^6(n+1)s \rightarrow np^5(n+1)s^2$ excitations of Na ($n=2$), K ($n=3$), Rb ($n=4$), and Cs ($n=5$), setting aside the case of Li $1s^2 2s \rightarrow 1s2s2p$ excitations, which have a different symmetry. The series Na–Cs offers the simplest of monovalent metals, with a factor-of-3 variation of atomic volume, and a factor-of-4 variation in lattice Debye temperature $\Theta_D = \hbar\omega_D/k$, for outer-core excitations that all fall in the energy range 11–31 eV. Intermixing of conduction states derived from other atomic orbitals, as in the *s-d* admixtures of the noble metals, is absent in these simple metals although, as detailed below, the $np^5(n+1)snd$ locally excited *configurations* play a significant role in the spectra of Rb and Cs. Also, it is observed for Na and K that the core-hole lifetimes τ are sufficiently long that broadening may be studied at the 10-meV level. These desirable characteristics motivate the studies of alkali-metal core processes reported in this paper. The difficulty of handling the reactive alkali metals, their low characteristic lattice temperatures, and their poor alloying capabilities for related investigations are practical complications that must be accommodated.

The research reported below uses emission spectroscopy to study the outer-core processes of alkali metals. Sodium was one of the metals first examined by Skinner[2] half a century ago, and has been investigated several times since then.[1] Accurate investigations of potassium metal were reported in the 1970s by Norris[3] following the observations of emission by Kingston[4] and Crisp *et al.*[5] The progressively more difficult cases of Rb and Cs core emission are reported for the first time in the present research.[6] Emission methods offer the advantages of high resolution from a front-surface probe that can be adapted to ultrahigh vacuum (UHV), to the necessary low sample temperatures, and to the need for sample preparation *in situ* by molecular-beam methods. Emission ordinarily probes several hundred Å below the surface, and, being thus free from the surface specificity associated with electron spectroscopies in the energy range below 1 keV, is well suited to alloy studies. The method nevertheless offers sufficient sensitivity to make emission from surface or interface features visible, as we demonstrate in what follows. Emission is the process exactly complementary to photon absorption. It is unique as a probe of the electronically relaxed and neutral excited state.

A variety of solid-state phenomena influence the widths of core transitions; some have been investigated for light alkali metals. The outer-core-hole decay rates, $W=\tau^{-1}$, of metals are determined by Auger processes whose rates exceed photon-emission rates by several orders of magnitude.[7] Figure 1 shows these decay processes

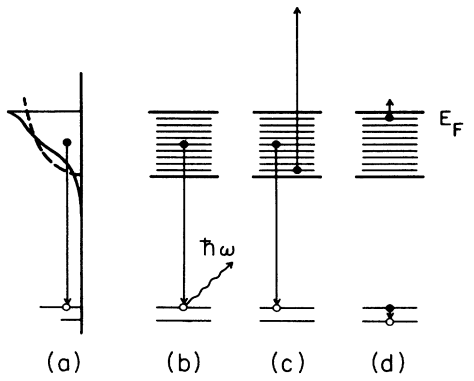

FIG. 1. Sketches showing (b) photon emission, (c) Auger decay, and (d) Coster-Kronig decay for a spin-orbit-split core p level analogous to that of the alkali metals. In simple theories the emission spectrum resembles the conduction-band s-state density [dashed line in (a)]. In real cases a "many-body" peak is seen at E_F and the band bottom is smeared by the lifetime of the band hole in the final state [solid line in (a)].

schematically. Lifetime widths of ~ 20 meV for Li (Ref. 8) and 10 meV for Na (Ref. 9) and 15 meV for K (Ref. 10) have been deduced from various considerations. Successive theories for Na, following the initial formulation by Morita and Watabe,[7] have predicted core-decay rates of ~ 3 meV,[7] 10 meV,[11] 1000 meV,[12] and 10 meV.[13] Such variations in the predictions leave uncertain expectations. As yet, for example, there is no indication from theory how the core lifetime might vary through the alkali series Na–Cs of similar metals. The experiments reported below reveal this behavior for the first time.

Two further broadening mechanisms are phonon creation and thermal blurring of the Fermi edge. The second of these, specific to metals, is discussed below. Phonon broadening of optical transitions in metals, like that in insulators, arises because the ground and excited states of a given core couple differently to nearby atoms. Early work[14–16] identified phonon broadening as important for the Li 1s core width, particularly electron-yield experiments by Kunz and co-workers,[15] and a phenomenology by Flynn[16] made the widths broadly predictable, including excess recoil broadening in electron spectroscopies. Specific predictions for alkali metals are given by Hedin and Rosengren[17] and the subject is summarized by Almbladh and Morales.[18] While the phonon theory appears to possess at least semiquantitative accuracy, definitive experiments are lacking, except for Li, mainly because low temperatures are required. A complication occurs when the hole decay rate τ^{-1} is comparable to the Debye frequency ω_D.[19–21] For $\omega_D\tau \gg 1$ the usual Stokes shift of insulators occurs, whereas for $\omega_D\tau \ll 1$, as in most metals, there is no shift. The deduced τ of Na,[9] mentioned above, comes from a measured shift between absorption and emission for $\omega_D\tau \sim 1$, using a theory of Almbladh.[21] The present work offers more direct measures of the lifetimes τ and phonon widths for several alkali metals.

If the conduction band remained undeformed, the core-hole recombination spectrum would image the density of band states. Friedel[22] recognized that in reality the band states deform locally to screen the core hole. Observed absorption and emission spectra nevertheless generally resemble conduction-band models, with sharp Fermi edges, but with added, sometimes sizable, anomalous peaks at E_F and with a large smearing of the band bottom in emission (see, e.g., Fig. 1). The energy-dependent lifetime of the *band* hole left by the recombination event causes the latter phenomenon;[2,1] the "Mahan–Nozières–De Dominicis (MND) anomalies" at E_F are associated with electron-hole pairs created by the shock of the optical event.[23,1] Analogous effects are clearly apparent in exact optical matrix elements of simple determinantal models in which a locality of the electron gas is suddenly deformed, as in screening of a core hole.[24] Asymptotic theories for the singularity by Mahan and Nozières and De Dominicis[25] are widely recognized. The theory permits a semiquantitative modeling of experiment in many cases. For example, the relevant partial state density, together with a fitted MND anomaly and band-bottom broadening, give a convincing description of the overall Na and K emission band shapes. Fits are generally less satisfactory for the polyvalent, but still simple, metals Mg and Al,[26] where the larger electron densities should favor Hartree-Fock predictions. Of special interest in the present research is that the low-density metals Rb and Cs have been thought to approach the Mott transition to the insulating state,[27] and that the resulting effects on the emission line shapes remain to be determined.

With this background, the present work was undertaken to determine for the first time in an isoelectronic series of simple metals how the overall band shape varies with atomic size, whether or not the phonon broadening can be systematically understood, and how the core-hole lifetime depends on the principal quantum number of the core. These questions provide the main focus for the research reported below. Section II describes an apparatus built to examine core emission from samples prepared *in situ* in ultrahigh vacuum, and for temperatures from 20 to 300 K. Certain essentials of data reduction are also described in Sec. II. An illustrative selection of spectra taken with K, Rb, and Cs samples is presented in Sec. III. In Sec. IV the results are analyzed and discussed in terms of current models of core processes in metals. A brief summary is provided in Sec. V.

II. EQUIPMENT AND DATA REDUCTION

In this section we first describe an apparatus constructed for the measurement of vacuum-ultraviolet (vuv) emission. The procedures employed to reduce the data to a useful form are then discussed.

A. Apparatus

Photon emission from core-excited metals is weak in the vuv energy range of 5–30 eV because fast Auger processes short-circuit the photon-decay channel. Two

features of the present experiments present further problems that make careful attention to overall apparatus design essential. First, temperatures down to 15 K are needed in order that temperature-dependent phonon broadening can be explored. Second, samples must be prepared and examined in the same vacuum chamber so that reactive materials remain free from surface contamination.

A reasonably sized cold-finger device capable of reaching 10 K can accommodate about 100 mW of excess power input from the electron beam used to excite core transitions. This corresponds to only 50 μA at a typical beam voltage of 2 kV. To obtain maximum brightness at the detector this beam must be optimally focused. Rough calculations suggest that for a spot size 50×500 μm^2 on a good thermally conducting substrate this heat load can be dissipated effectively at low temperatures. In our chosen experimental design, light is accepted from this source at $f/0.5$ using an ellipsoidal mirror with a 10:1 focal-length ratio to match the source into the entrance slit of an $f/4.5$ McPherson 234 vuv monochromator. The resulting 0.5×5-mm^2 illumination of the monochromator entrance slit was generally consistent with the required light-collection efficiency and resolution. The ellipsoidal mirror was plated with Pt to ensure a reasonably high and smooth reflection efficiency through the photon energy range up to 30 eV.

A Perkin-Elmer electron gun was adapted to the system as the excitation source, with a homemade relay lens mounted 0.25 in. above the sample surface to improve the focus on the substrate. The substrate was a 1-mm-diam copper rod supported by sapphire blocks. This provided the thermal conductivity at low temperature required to dissipate the heat load from the electron beam. About half the accelerating voltage was supplied between the lens and the rod, so that the electrostatic field of the substrate provided additional focusing. Each run started with a procedure designed to obtain an optimal focus of the electron beam on the substrate rod. The location of the substrate rod and mirror was adjusted such that the image of the irradiated spot on the substrate fell accurately on the monochromator entrance slit.

Figure 2 shows the experimental layout made possible by these arrangements. A Helitran cold finger connected to a Cu can was introduced into the vacuum chamber through a stainless-steel collar bolted above a six-way ultrahigh-vacuum UHV cross. Above the collar, isolated by a gate valve, the monochromator was suspended with its own ion pumping, as shown. The Helitran-cooled can contained the substrate, the electron lens, and the focusing mirror. A UHV x,y,z translation stage on which the can was mounted allowed the sample to be so positioned that the image of the illuminated spot coincided with the monochromator entrance slit. The substrate itself was mounted on a crossbar fixed rigidly above the mirror and adjusted to coincide with the first mirror focus prior to insertion of this assembly into the inner cryocan. The entire inner can was surrounded by a liquid-nitrogen-cooled thermal-screening can supported in a fixed position.

General access to the sample environment was provided by the six-way cross. An ion pump occupied one horizontal port, the electron gun a second, and a viewing port a third. The fourth horizontal port held sample-preparation facilities described below.

Electrical feedthroughs for monitoring the can and substrate temperatures and for focusing and deflecting the electron beam were made via ports on the Helitran cold finger. Calibrated carbon resistors and Chromel-Alumel thermocouples were used as thermometers.

The sample-preparation assembly was connected by a gate valve to the lower port of the six-way cross. On the lowest flange were mounted two molecular-beam sources for metals. The alkali-metal sources have been described elsewhere.[28] Sealed ampoules inserted into soft Cu containers could be broken in vacuum and evaporated through heated stainless-steel tubes. Each alkali-metal source was located at the entrance to a liquid-N_2-cooled (LN_2) Cu shielding tube that defined a direct path to the substrate region, and confined stray evaporants to a small surface area for ease of clean-up. The entire sample-preparation assembly on the lower flange was connected

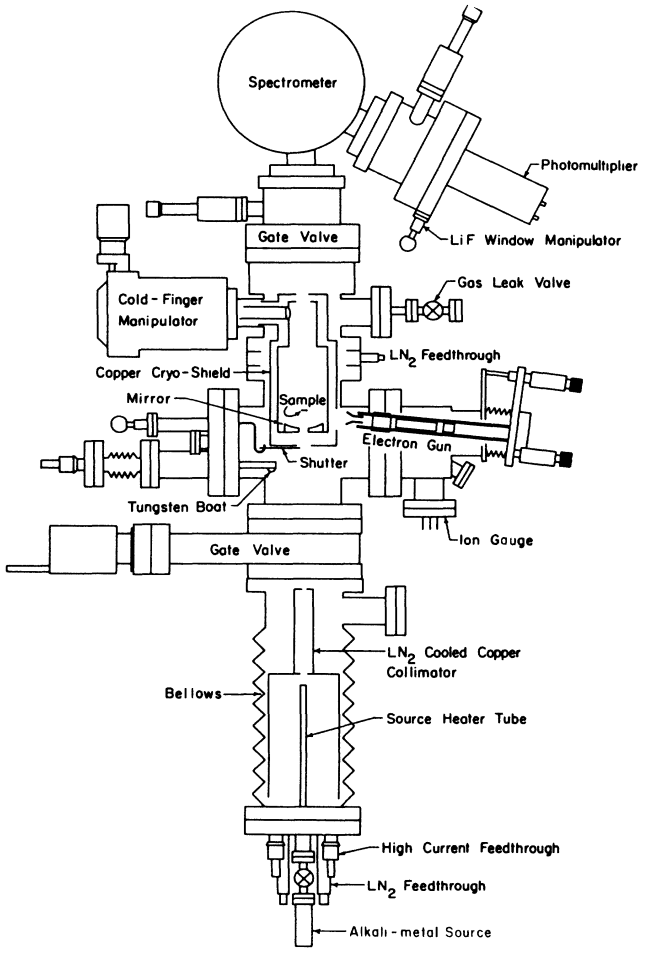

FIG. 2. Apparatus for emission experiment shown schematically. The photomultiplier detector and exit-slit assembly may be replaced by an array detector as described in the text. An ion pump is mounted on the back port of the sixway cross and another on the spectrometer.

to the apparatus above by a large bellows that allowed introduction of the assembly into the substrate environment for sample preparation and allowed its removal and isolation from the main chamber by the lower gate valve. The dual sources allowed alloys to be prepared. Samples containing gas impurities could also be prepared using a calibrated gas leak which enters the chamber through a port opposite the cold finger. These were employed in other research to be reported elsewhere.

In the actual arrangement, as sketched in Fig. 2, the molecular beams pass from the sources to the substrate through a hole in the center of the light-collecting mirror. This path was screened off after sample preparation by a shutter on the liquid-N_2-cooled outer can, activated by a linear-motion feedthrough on the fourth horizontal port of the six-way cross. Also accessed through this port was a retractable tungsten evaporation boat for an optically inert metal such as silver that could be used to decouple successive emission measurements, one from the next. The sample thickness was monitored by the frequency shifts of calibrated quartz crystals located on the inner cryocan adjacent to the molecular-beam paths to the substrate.

In summary, pure metal or alloy films could be prepared *in situ* in UHV at temperatures from 15 K upward on Ag- or Li-covered surfaces that, for emission purposes, were only weakly active. Typical ambient pressures in the 10^{-10}-torr range were achieved after bakeout, rising to the mid-10^{-9}-torr range during sample preparation (10^{-8} torr for Li), and falling back to the 10^{-10}-torr range after evaporation. At low temperatures the pressure inside the cryocan must be much lower owing to strong cryopumping by the inner can.

Good thermal contact was maintained between the thermometers (carbon resistor and thermocouple) and the sapphire, but no way of directly monitoring the temperature at the electron-beam focus was available. Rough estimates indicated that the temperatures there were less than 1 K higher than that of the sapphire. Cs spectra (the worst thermal conductor) at 20 and 200 K showed no significant change when the beam was defocused to decrease the power density. Thus, the low-temperature arrangements appeared to be effective.

For most of this research the light reaching the monochromator exit slit was monitored using a CsI-coated EMI 9642/2B phototube and photon-counting techniques. The approximate efficiency defined as the ratio of photons emitted to photons detected was about 10^{-4} at 15 eV for 2-Å resolution and varied as the square of the resolution. This is probably 10^2 times brighter than conventional soft-x-ray–emission (SXE) systems that employ grazing-incidence optics. More recently, for work in the energy range $\hbar\omega > 9$ eV we have installed an array detector using a CsI-coated microchannel plate optically coupled to a RCA charge-coupled device detector. By detecting an entire spectrum at one time, this system has a linear inverse dependence of count rate on resolution and increases the detection efficiency by a further factor that may reach ~ 30. These methods make fluorescence from surface species or impurities at the 1% level accessible for metals. In the present experiments, excellent signal-to-noise ratios for pure metal films down to a few monolayers in thickness could be obtained by scanning with a phototube detector. Most of the spectra reported in what follows were obtained by these means.

The spectra are nevertheless distorted by the light-collection process and they require corrections described in what follows.

B. Data handling

Both the photomultiplier detection and array detection systems gave digital outputs by standard methods. Here we discuss signal optimization and necessary data processing. Observed intensities were first reduced to functions of photon energy, using the overall detection efficiency and spectrometer calibration. Further procedures were needed to correct the spectra for self-absorption of emitted photons in the sample. The work of Crisp[10] and others has established that these effects can cause significant distortions in thick films. It is also necessary on occasion to remove background signals, spin-orbit partners, etc., as summarized here.

Remote control of data acquisition with the photomultiplier tube and photon-counting electronics was achieved by computer control of the timer, scalers, and the spectrometer drive stepping motor. To eliminate random processes such as electron-beam drift, the data collection was box-carred by automatically sweeping the scan 20–50 times with dwell times of typically 1–10 sec per point. This yielded signals that were shot-noise limited.

Data acquisition with the array detector required a different approach. The 640×1024 pixels, each 15×15 μm^2, were electronically binned into 1×32 "superpixels," and spectra obtained by summing the 16 superpixels along the effective slit length. Spectra so acquired are distorted by sensitivity variations from one pixel to another. A "dark field" was subtracted to eliminate the offset inherent in the charge coupled device and the flat field response then divided out, using an image in which the spectrometer repeatedly swept a strong band over the relevant region. This procedure eliminates detector-gain variations over the chosen energy band. Cosmic rays caused additional sharp spikes in images acquired by these means when the scan times exceeded a few minutes. Longer scans were therefore broken into short intervals for which cosmic-ray spikes could be identified by their large size and random locations, and eliminated before the parts were summed to obtain the desired signal.

Several related points are worth noting in connection with array detection. Flexible operation required that the dispersion in Å/per pixel be determined for several grating positions. In the present case this was accomplished using atomic spectra from gaseous Ar, Kr, and Xe. Spectra about 450 Å wide could be taken. Wider scans were patched together from data acquired at different grating positions. The shifted images also provided a useful check that an observed spectral feature was not an artifact caused by a detection-gain anomaly. The gap spectra were also used to check the monochromator resolution. As the atomic-emission lines had nearly the same width as the zeroth-order line, the latter was subse-

quently used to monitor the instrument resolution when recording alkali-metal spectra.

Raw data were converted directly to functions of energy, scaling the intensity as E^{-2} to eliminate the distortion of constant-*wavelength* resolution inherent in the spectrometer. Corrections for optical-efficiency variations through the light-collection and dispersion optics proved a difficult task. For the region above 12 eV an effective expedient was to use the transition radiation and bremsstrahlung of electron-excited Li metal as an efficiency monitor, since Li has no strong interband excitations in this region. Prominent features in the Li scans also appeared in similar scans of Cu and Au, thereby confirming their origins as artifacts caused by the optics themselves. Below 12 eV the Li transition radiation increases sharply and this method was no longer useful. It was nevertheless verified that sharp instrumental features are absent from the (9–12)-eV region of our Cs spectra, and these data are presented without further correction. Optical efficiency remains a serious problem for emission measurements in the photon-energy range 10–30 eV, in part of mitigated by our present interest in narrow bands. A substantial but smooth gain variation even by 10% over a 2-eV band does not cause a large change of normalized shape, as illustrated for model bands in Fig. 3. Smooth variations cause still fewer problems through the 200-meV range relevant to the Fermi-edge–broadening studies described below. For these purposes, the use of observed instrument-induced irregularities from an otherwise smooth spectrum to eliminate similar features from unknown spectra is a useful procedure. In particular, a spurious dip in the raw data for Rb emission near 14 eV was eliminated by these means.

Reabsorption of emitted photons is important because the signal strength is improved by use of thick films in which, however, reabsorption occurs. In practice, these effects are often significant for films greater than 200 Å thick. Our procedures made use of the alkali-metal absorption coefficients reported by Sato[29] *et al.*, and the ionization efficiency as described by Crisp,[30] to calculate a correction factor that depended on the photon energy. Details of these procedures are given in the Appendix. The results turned out satisfactorily. To illustrate the equipment efficiency with the phototube and also the use of reabsorption corrections, Fig. 4 shows the emission from K films with thicknesses between 2200 and 320 Å. The signal-to-noise ratios are excellent, but there is an apparent variation with film thickness of the spin-orbit partner intensity ratio. Figures 4 and 5 show these same

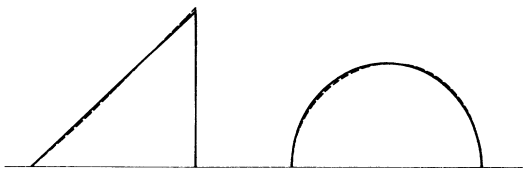

FIG. 3. Sketches showing the type of band distortions (dashed lines) caused by a smooth 10% increase of gain across a normalized band (solid lines).

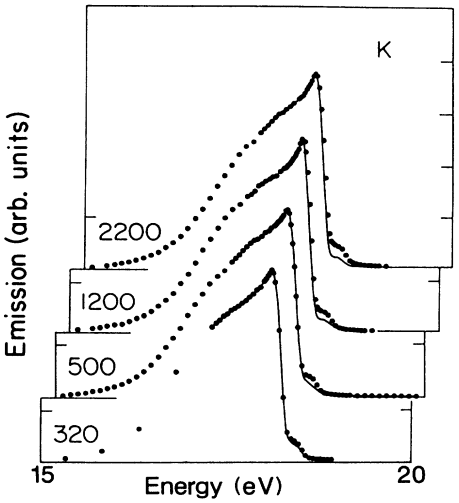

FIG. 4. K spectra (lines) as a function of film thickness (indicated) at 20 K. Reabsorption causes the observed changes with thickness (see Fig. 5), which are largely eliminated (points) by the procedures described in the text.

data corrected for reabsorption. The corrected spin-orbit partner intensity remains rather constant from 2200 down to 150 Å, where reabsorption becomes negligible.

The apparent growth of the $J=\frac{1}{2}$ partner emission in films less than 150 Å thick is a separate matter of considerable interest. After making the initial observations, we confined much of our K work to films 100 Å thick or less,

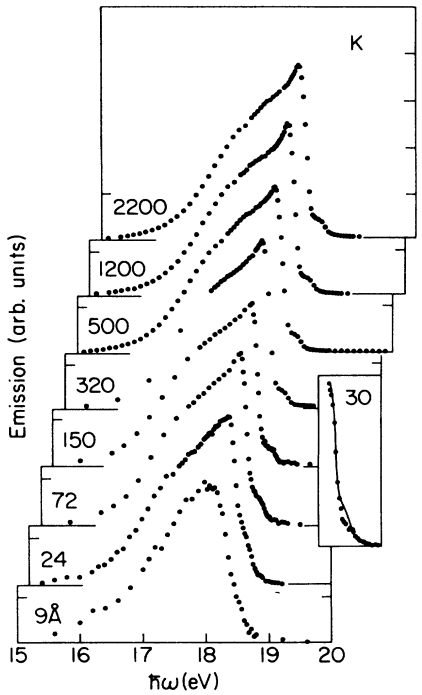

FIG. 5. K spectra corrected for reabsorption. Films below 200 Å thick have a negligible reabsorption corrections. Inset shows how a Li overlayer eliminates (data points) the apparent change of $P_{1/2}$ to $P_{3/2}$ intensity (line) associated with the free K surface in the thinner films.

expecting that reabsorption required this constraint. The mistake was made less easy to avoid by the fact that the observed intensity ratios of the spin-orbit partners in emission are highly anomalous (see Secs. III and IV). In fact, this emission is a surface-induced feature that happens to fall near the $J=\frac{1}{2}$ core-edge position. In the inset of Fig. 5, a Li overlayer on a 30-Å thick film is seen to eliminate much of the surface emission and to restore the $J=\frac{1}{2}$ process to its size in thicker films. The problem thus arose from the high equipment sensitivity which made emission from surface K atoms unexpectedly visible. The same surface feature in K has recently been detected by Jensen[31] using photoemission. In the present work we have observed similar effects in very thin Cs and Rb films also, with the surface edge again blue-shifted from the main bulk process by ~ 0.2 eV. Section IV A offers brief interpretative comments about these shifts. We find that all such surface emission is generally quenched by a foreign metal overlayer, and this procedure was used in the present research once the problem had been identified.

Small reabsorption corrections were routinely made for the Cs and Rb results reported in Sec. III. For K films 70 Å thick, no such corrections were needed, as Figs. 4 and 5 make clear. Unfortunately, the K edge is broadened in the thin films, so that the natural bulk edge width was not observed. As a result, our later discussion of the bulk signals relies on a small fraction of the total data.

For many purposes it is useful to deal with a single core process, in which case the elimination of background and spin-orbit partner emission becomes desirable. Emission from the underlying substrate frequently contributed to our observed spectra, and it was therefore measured prior to film preparation and subsequently subtracted. Other smooth background emission arose from processes in the film itself and therefore could be eliminated only by estimating its interpolation under the band of interest. For the spin-orbit partner emission we assumed a shape identical to that of the main band and performed running subtractions with the spin-orbit splitting and intensity ratio as free parameters. These were optimized by seeking to eliminate the intensity oscillations that arise for incorrect choices of parameters. In all cases studied the deduced splitting agreed with the atomic value to within the uncertainties. A number of studies were limited to the Fermi edge alone so that running subtraction became impossible. In these cases a separate spectrum was shifted and scaled appropriately so that a satisfactory best subtraction could be made.

III. RESULTS

This section gives representative results for the outer-core emission spectra taken from solid films of K, Rb, and Cs. Full band spectra of these three metals are presented first, followed by Fermi-edge measurements taken at temperatures 20–300 K, and finally relative emission intensities of the three metals.

Shown in Figs. 6, 7, and 8 are the emission-band profiles of the heavy alkali metals K, Rb, and Cs, respectively. These spectra were taken at 20 K or below with

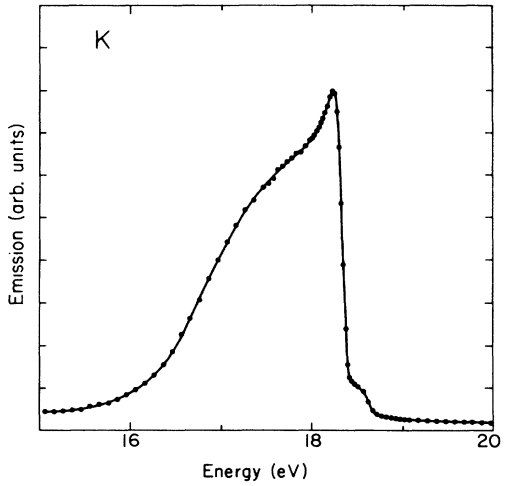

FIG. 6. Band spectrum for K 1200 Å thick with an overlayer of Li. Spectrometer resolution was 85 meV. The spectrum is corrected for self-absorption and instrumental response.

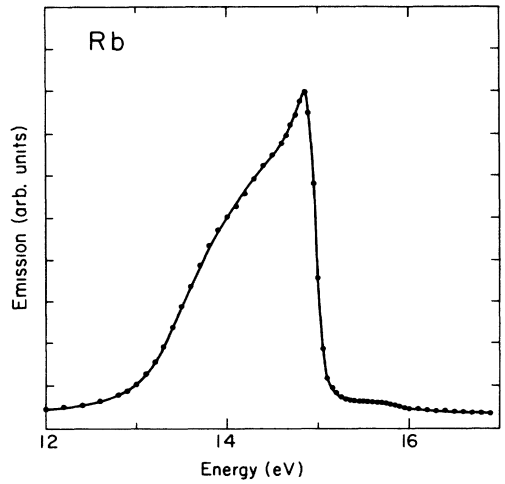

FIG. 7. Band spectrum for Rb 400 Å thick with an overlayer of Li. Spectrometer resolution was 0.12 eV. The spectrum is corrected for self-absorption and instrumental response.

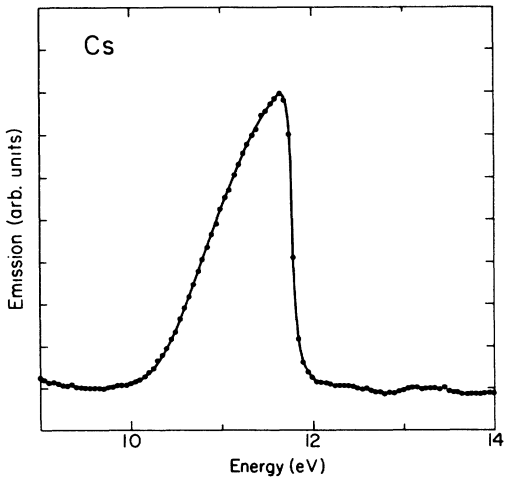

FIG. 8. Band spectrum for Cs 700 Å thick with an overlayer of Li. Spectrometer resolution was 50 meV. The spectrum is uncorrected for spectrometer response. It is not certain that feature at 13.5 eV is the $P_{1/2}$ band edge.

the phototube detector (see also Figs. 4 and 5 for K). They are corrected for spectrometer response and self-absorption as described in Sec. II. Each sample was covered by a thin overlayer of Li metal to suppress surface emission (see Sec. II). The threshold energy could be established within a calibration uncertainty of ~ 30 meV. Samples were typically prepared at 77 K and thereafter subject to a variety of temperature cycling. No systematic dependence of edge position or shape on thermal history was ever established. This was also true for samples prepared initially at liquid-He temperatures.

The $J=\frac{3}{2}$ emission-band edge of K is shown in Fig. 6, and the $J=\frac{1}{2}$ spin-orbit partner emission-band edge, a factor ~ 10 smaller, is blue-shifted from it by 0.27 ± 0.01 eV. This is consistent with the spin-orbit splitting of atomic K (0.26 eV),[32] and solid K observed by absorption[33] (0.26 eV), and by inelastic electron scattering[34] (0.27 eV). Crisp reports comparable values of the emission results for K.[10] The spectrum is strongly broadened at the band bottom and some many-body enhancement of emission strength is visible immediately below the Fermi-energy edge. The bandwidth is roughly the free-electron Fermi energy of solid K, and the shape is in general agreement with earlier reports by Norris.[3] A more quantitative discussion of alkali bandwidths is given in Sec. IV.

The emission bands of Cs and Rb show characteristic band shapes similar to K. However, the strength of the many-body enhancement below threshold and the strength of the spin-orbit partner emission weakens progressively for Rb and Cs. The emission-band widths also decrease as expected with decreasing E_F.

An unexpected observation is the striking loss of the $J=\frac{1}{2}$ spin-orbit partner intensity in Rb and the lack of any confirmed $J=\frac{1}{2}$ emission in the Cs spectrum. The weak spin-orbit partner band for Cs we described in an earlier brief report[6] coincides with a small anomaly in the reflectance of the optical components and cannot now be regarded as established with certainty. The Rb emission spectrum shows a spin-orbit splitting of 0.88 ± 0.02 eV as compared to 0.844 eV for atomic Rb.[35] For solid Rb observed in absorption the $J=\frac{1}{2}$ hole level overlaps the d excitation (Sec. I) and its energy cannot be distinguished separately.[33] The splitting in atomic Cs has been measured[36] as 1.76 eV, but we have not observed the corresponding solid-state process unambiguously.

High-resolution studies of the Fermi edges at various temperatures reveal that the edge widths and threshold energies both increase with temperature. A detailed examination shows that the shape of the Fermi edge changes as its width increases. Specific profiles for K, Rb, and Cs are presented in Sec. IV, where the observed profiles are compared with fitted models. Figure 9 illustrates the general edge-width behavior for the three metals through the dependence of the 25–75 % widths on $T^{1/2}$, including earlier results by Tagle *et al.*[37] on K-edge widths for comparison with the present data. The longitudinal Debye temperature is indicated for each of the metals. The edge widths are not corrected for instrumental resolution of 45, 32, and 40 meV full width at half maximum (FWHM), respectively, for K, Rb, and Cs.

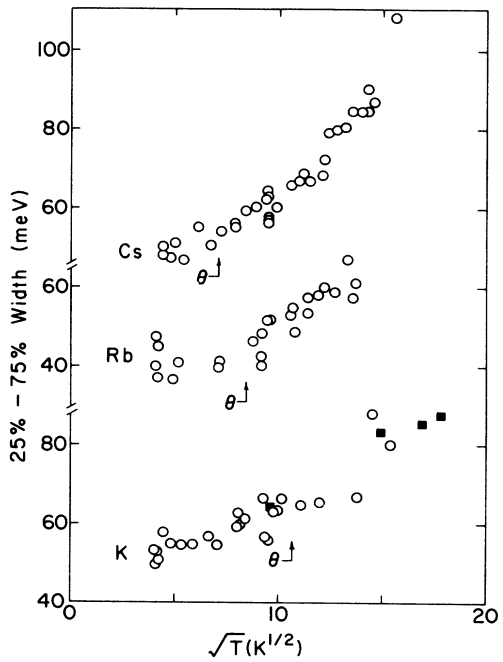

FIG. 9. 25–75 % edge widths for K, Rb, and Cs, uncorrected for resolution and reabsorption. Longitudinal Debye temperatures are indicated by arrows marked Θ. Data from Tagle *et al.* (Ref. 39) (squares) were taken with 64-meV resolution on thick films.

second moments of these resolution functions exhibit only small deviations from those of Gaussians with the same FWHM.

Below the respective Debye temperatures, Θ_D, the edge widths tend to show little temperature dependence. Above Θ_D, the widths increase more rapidly. Two relevant broadening mechanisms are photon broadening, which is expected to increase the edge width as $T^{1/2}$

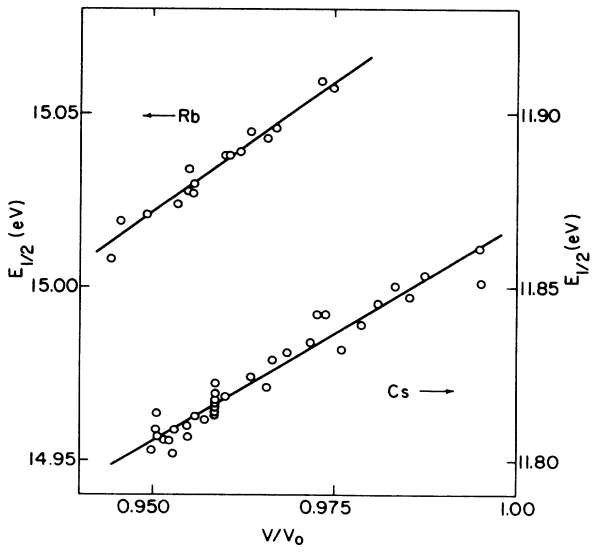

FIG. 10. Energy of midpoints of edges as functions of the relative volume with thermal dilation for Rb (top) and Cs (bottom). Absolute energy scales are uncertain by 30 meV. V_0 is the volume at room temperature, zero pressure.

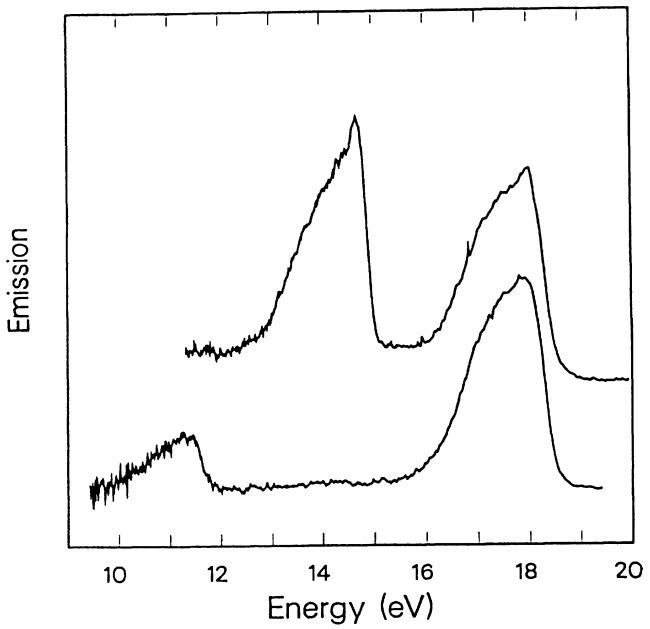

FIG. 11. Emission from bilayer films. Top, 35 Å of K on 47.5 Å of Rb; bottom, 44 Å of K on 38 Å of Cs.

above Θ_D, and Fermi-edge thermal blurring proportional to T. A detailed analysis of the edge spectra is given in Sec. IV.

Figure 10 shows the measured threshold energies as functions of the relative volumes for solid Rb and Cs. Similar data published earlier[37] for Li, Na, and K exhibit a linear dependence of threshold energy on thermal dilation of the lattice. The present results exhibit a similar trend. Values of the relative volumes as functions of temperature were taken from Refs. 38 and 39.

Much interest attaches to absolute values of the core-hole decay rates. In an effort to investigate these effects and their variation through the series of alkali metals, we have made measurements of the relative intensities of emission from K, Rb, and Cs. The experiments were performed on films less than 50 Å thick. To eliminate light-collection efficiencies that could vary somewhat from one experiment to the next, we observed emission from the two metal films *simultaneously,* in the same spectral measurement, with the alkali metals grown one on top of the other in pairs. The films were kept thin to avoid self-absorption and electron-attenuation effects.[40] Examples of spectra for K-Rb and K-Cs pairs are presented in Fig. 11. From measurements of the areas under the emission bands in such spectra, the relative emission intensities per atom for K:Rb:Cs were determined as 3.9:3.2:1.0. These figures include the excitation cross sections; the ratios of areas alone are 2.3:2.5:1.0.

IV. DISCUSSION

In this section we analyze the overall emission-band profiles, the Fermi-edge broadenings, and the observed spin-orbit partner characteristics.

A. Alkali-metal band shapes

The spectra presented in Sec. III reveal strong similarities among the emission-band shapes of the different alkali metals. To make small departures from the average more apparent, we present in Fig. 12 superposed spectra of K, Rb, and Cs. The spectra are normalized in area and each is scaled in width by a factor E_0 chosen to make the different results fall close to a common average shape. Also included are data for Na from Crisp and Williams[41] and from Callcott *et al.*[9] The alkali-metal emission-band shapes are remarkably similar. Small but systematic differences are also visible, most noticeably in the character of the small peak near threshold (at E_F). The peak is largest for Na and appears to dwindle through the series of alkali metals until for Cs it is no longer visible.

To show how the observed spectra compare with theory, Fig. 13 compares the observed K band shape with a theoretical band density of s states for K, as calculated by McMullen.[42] A comparable theory for Na by Gupta and Freeman[43] is also given, appropriately scaled in energy. It shows that changes in band structure from one alkali metal to the next are rather small. The dashed line is the theoretical curve for Na when broadened by convolution with an energy-dependent Lorentzian with the width variation predicted by Hedin,[44] but scaled to fit the experimental lifetime reported by Jensen and Plummer[45] for the band bottom. This broadening simulates the effect of the *band*-hole lifetime in the final state (i.e., without the core hole). It is clear that the combination of band theory and quasiparticle lifetime broadening provides a satisfactory semiquantitive description of the band shapes except near the Fermi edge. This basic picture is further confirmed by the empirical bandwidth-scaling factors employed for Fig. 12 and collected in Table I. The ob-

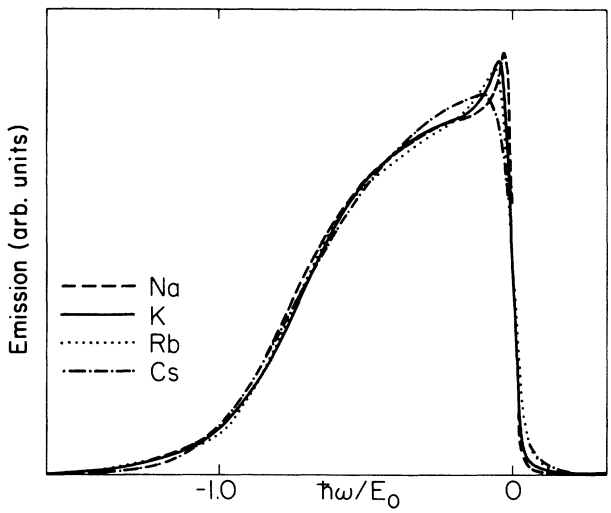

FIG. 12. Normalized emission intensities for Na, K, Rb, and Cs. Band energies are scaled by a factor E_0 (see Table I). All spectra are scaled by E^{-5} to account for phase-space and spectrometer-sensitivity factors. The Na spectrum is a combination of the full band spectrum from Crisp and Williams (Ref. 41) and more recent edge data from Callcott *et al.* (Ref. 9).

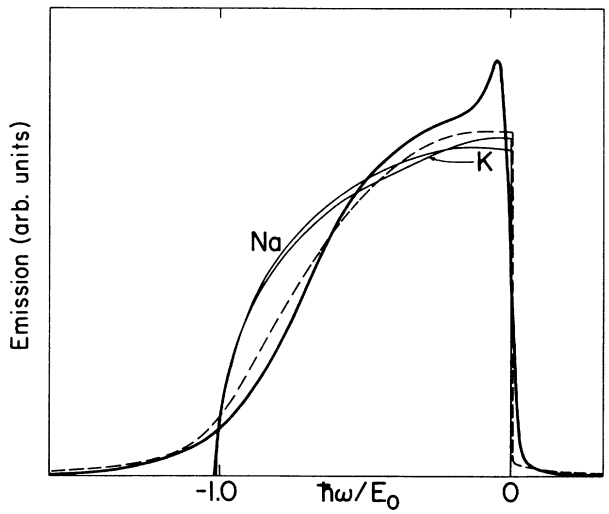

FIG. 13. K emission (thick line) compared with predictions for K (Ref. 42) and Na (Ref. 43) (thin lines). Dashed line is a theoretical curve for Na broadened by final-state lifetime broadening (Refs. 44 and 45).

served widths track quite accurately with the known Fermi energies, also given in Table I. It is expected from theory that the lifetime broadening of the final state should increase approximately as the bandwidth,[44] and this may help to explain the similarities among the different alkali-metal band shapes. Very recently, the theory of the alkali-metal bandwidths has been revised by new self-energy calculations,[46] that agree with the latest photoemissions experiments.[45] The corrections are quite substantial, but give much the same fractional change for the different alkali metals. Therefore they do not modify our arbitrarily scaled comparisons between observed "bandwidth" E_0 and the free-electron E_F significantly.

In point of fact, the one-electron band structure in Fig. 13 is far removed from any realistic description of the recombination event because the presence of a localized core hole severely distorts the conduction-electron distribution in its immediate vicinity.[22,1] Thus the core hole is filled by an electron having a strongly perturbed wave function, so that corresponding changes of the emission profile are expected. It is important that the similarity among the various alkali-metal band shapes should be retained despite these complications.[1] The conduction-electron distribution near a core hole in Na should resemble that near Mg in Na, according to the reliably accurate "$Z+1$ model"[47] just as that in Cs must resemble Ba in Cs. These two systems are identical in coarse Coulombic structure and differ mostly by small pseudopotential features, other than in the Na and Cs atomic volumes

TABLE I. Emission-band widths for alkali metals: E_0 is the scale factor used in Fig. 12 and E_F is the free-electron Fermi energy.

	Na	K	Rb	Cs
E_0 (eV)	3.16	2.22	2.01	1.49
E_F (eV)	3.24	2.12	1.85	1.59

(i.e., in E_F). It is therefore a quite general expectation that the alkali metals should have similar recombination spectra that scale as E_F, to the extent that one-electron behavior is principally involved. Figure 12 may be regarded as the experimental verification of these broad and model-independent ideas.

The small peak observed near E_F has been widely discussed and attributed to electron-hole–pair creation caused by the shock of the sudden change of interactions in the optical event.[23,1] From an empirical standpoint these effects appear to be systematically smaller in emission than in absorption, and smaller for heavy alkali metals than light ones. The absorption data of Sato *et al.*[29] and Haensel *et al.*[48] are reproduced in Fig. 14 for convenience in making these comparisons. Only a rounded maximum is visible for Cs emission, although a distinct peak remains for Rb. Asymptotic predictions for this (MND) behavior are referred to in Sec. I. Simple model calculations[24] carried through accurately in a Δ self-consistent-field (ΔSCF) approach to the core-hole effect exhibit both a peak near E_F and some (nonlifetime) rounding near the band bottom. Thus the predicted emission results bear a semiquantitative relationship to the observed band shapes. ΔSCF calculations that model the individual metals and their core holes for complete spectral predictions are lacking. Thus, it is not clear at present whether or not the absence of a peak for Cs is related to the progressive dominance of Coulombic forces as the size of the metallic cell is increased. A more detailed understanding of these small line-shape features must await realistic theoretical predictions.

Rosengren and Johanssen[49] have employed the $Z+1$ model to estimate the shift of the core-excitation threshold for surface atoms. For completeness we summarize the present knowledge for alkali-metal surfaces here. Table II lists the energy shifts observed in the present research for surface sites of Cs, Rb, and K, together with the photoemission values by Jensen[31] for K and by Kam-

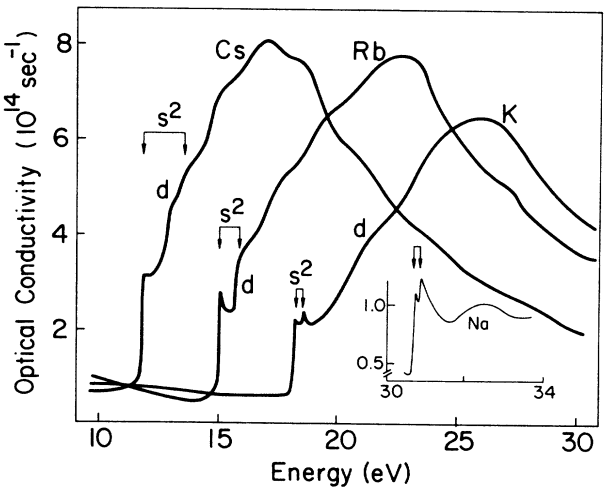

FIG. 14. Absorption spectra for Cs, Rb, and K from Sato *et al.* (Ref. 29) as reported by Miyahara *et al.* (Ref. 33). Inset shows Na absorption from Haensel *et al.* (Ref. 48) scaled to the data from Miyahara *et al.* Atomic level splittings are indicated.

TABLE II. Surface core-level shifts (in eV) for the alkali metals. Experimental uncertainties are ±20 meV.

	Na	K	Rb	Cs
Expt.	0.22[a]	0.23[b,c]	0.24[b]	0.24[b]
Theor.	0.220[a]			

[a]Reference 50.
[b]Present work.
[c]Reference 31.

merer *et al.*[50] for Na. The latter authors use density-functional theory to obtain the $Z+1$ model energy shift for surface atoms as 0.2 eV for Na. There are indications from measured surface energies that the surface effect should have a similar magnitude for the different alkalis,[51,50] which is consistent with the experiments cited in Table II.

B. Temperature-dependent edge profiles

The emission edges of K, Rb, and Cs shown in Sec. III are significantly wider than the equipment resolution, and the excess broadening is temperature dependent. In what follows the broadening is modeled to identify the main mechanisms responsible for the observed widths.

Two lifetimes contribute to the line shapes. First is the core-hole lifetime τ of the excited initial state, which convolves the line shapes with a Lorentzian of width $\hbar/\tau$. The second effect is the quasiparticle lifetime in the final state. This procedure little edge broadening because the lifetime diverges at E_F, but the summed effects of deeper holes do produce a finite background-like emission above E_F that must be taken into account.

In one-electron theory the Fermi-edge broadening is described by the Fermi-Dirac distribution. More generally, finite-temperature calculations[52] within the MND theory show that an "effective temperature," which involves the MND exponent α, must be employed. The present calculations use the value of α deduced from absorption studies by Ishii *et al.*[33]

Finally, the interaction with the phonon system causes a temperature-dependent "phonon broadening" of the emission edge. For $\omega_D\tau \ll 1$, with ω_D the Debye frequency, a Gaussian broadening is anticipated. Theories by Flynn[16] and by Hedin and Rosengren[17] predict the expected temperature dependence of the Gaussian width, and the phenomena are reviewed by Almbladh and Morales.[18] More complicated "incomplete relaxation" behavior that is not of immediate concern here has been predicted for cases in which $\omega_D\tau \sim 1$.

Our basic procedure was to simulate the band spectrum using a one-electron transitional density of states as calculated, for example, by Gupta and Freeman,[43] with a small peak superposed on it near threshold energy E_F. This profile was then modified by convolution with the broadening functions described above. All the results are insensitive to the precise form of the threshold peak. In this work we used the threshold peak $(E_t - E)^{-\alpha}\exp[-\lambda^{-1}(E_t - E)]$ for $E < E_t$, with $\lambda \sim 0.2$ eV and α chosen from the absorption results is Ishii *et al.*[33] The results are little affected by the details of these choices. The modified band with its peak was then broadened using an energy-dependent Lorentzian to represent the band-hole contribution of the final state. This basic spectrum, when convolved with the experimentally determined (essentially Gaussian) apparatus resolution function, was employed to identify the additional effects of the core-hole lifetime and phonon and Fermi-edge thermal-broadening processes. These procedures are reasonably practical, although the forms adopted for the basic band spectrum are somewhat arbitrary.

Detailed fits were performed for a tightly constrained model in which the core-hole lifetime was assumed to be independent of temperature, and the thermal broadening of the Fermi edge was that predicted by the finite-temperature MND calculations mentioned above. Abundant experimental spectra were merged near specific temperatures to obtain fewer curves with better statistics. A least-squares procedure was used to extract the best Gaussian widths required to fit the edge profiles, given particular choices of the temperature-independent core-hole lifetime. It was necessary to subtract a linearly varying background in order that the procedure worked effectively. From the fits, the optimum core-hole lifetime τ was selected as the value that best reproduced the expected *temperature dependence* of the phonon broadening, with the absolute *scale* of the phonon broadening a freely floating parameter. Figure 15 gives as points the fitted Gaussian widths for optimum choices of τ in the cases of K, Rb, and Cs. The lines through the points are the predictions of Hedin and Rosengren[17] using longitudinal Debye temperatures from neutron scattering[53] and

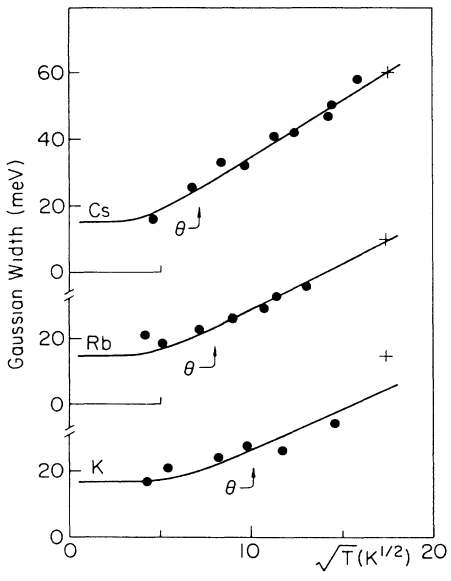

FIG. 15. Gaussian widths, σ, from fits to data with Lorentzian widths (FWHM) fixed at 50, 25, and 50 meV for Cs, Rb, and K, respectively. Lines show theoretical phonon widths of Hedin and Rosengren (Ref. 17); crosses are predictions for 300 K by Flynn (Ref. 16) Longitudinal Debye temperatures are indicated by arrows marked Θ.

with a free choice of the coupling constant. Also shown in Fig. 15 as crosses are the theoretical predictions by Flynn,[16] using no free parameters, for the room-temperature phonon widths of the three metals.

Figures 16–18 compare the observed edge profiles (points) with those predicted (lines), using the optimal hole-decay rates W, together with the *theoretical* phonon widths obtained from the fits in Fig. 15. Figures 16–18 show excellent fits between experimental data and the model. Furthermore, the phonon-broadening theory provides a good description of the way the Gaussian widths vary with temperature in Fig. 15. Both agree satisfactorily with the absolute room-temperature widths predicted by phenomenological modeling.[16] Thus, the entire set of data for each metal is well described by a tightly constrained model. There is good reason to have confidence in the Lorentzian-lifetime-related parameters and in the phonon-broadening contributions deduced from these fits.

Caution is nevertheless needed in the final assessment of the results. Experience with the procedures makes apparent that the data contain limited information about the threshold peaks and the effective Fermi-edge–width temperature, so that both these MND-related phenomena could probably be treated equally well by other models. Also, fits to the profiles for Cs when both the Gaussian and Lorentzian components were allowed to float freely did *not* indicate unambiguously that the lifetime component remained independent of temperature. Rather, there was a tendency for τ^{-1} to increase with T for Cs, whereas for K and Rb no such trends could be detected. In short, while the overall fits to the model lend substantial confidence to the global interpretation, the analysis does not, for example, establish that the core-hole lifetime is indeed temperature independent in all cases. We believe that the limitations of multidimensional fits of this type to edge spectra require wider recognition.

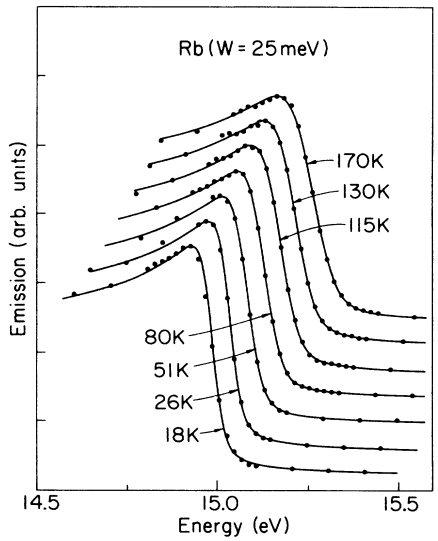

FIG. 17. Fit of edge-shape modeling (lines) for Rb to data (points) as described in the text. Results for different temperatures are offset for clarity. W is the lifetime Lorentzian width chosen for best fit to all data sets.

The example of K provides a case in point. As mentioned in Sec. II B, a misassessment of the self-absorption correction led us to perform most experiments on films about 70 Å thick. The data in Fig. 16 are consistently selected from this thickness range. They lead by the procedures detailed above to an estimate to an estimate of 50 meV for the core-hole–lifetime width. It is apparent

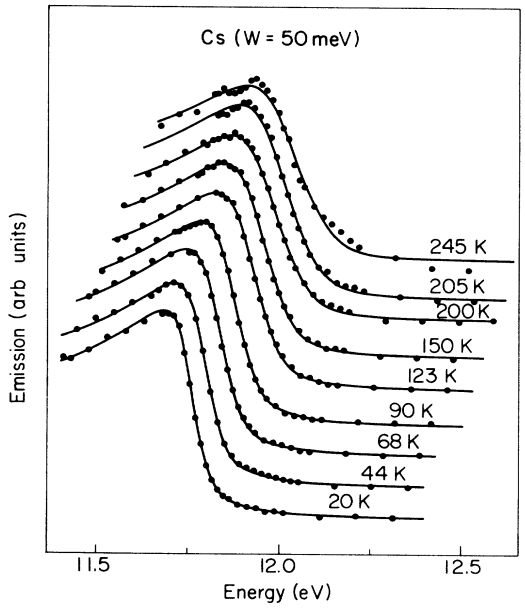

FIG. 16. Fit of edge-shape modeling (lines) for Cs to data (points) as described in the text. Results for different temperatures are offset for clarity. W is the lifetime Lorentzian width chosen for best fit to all data sets.

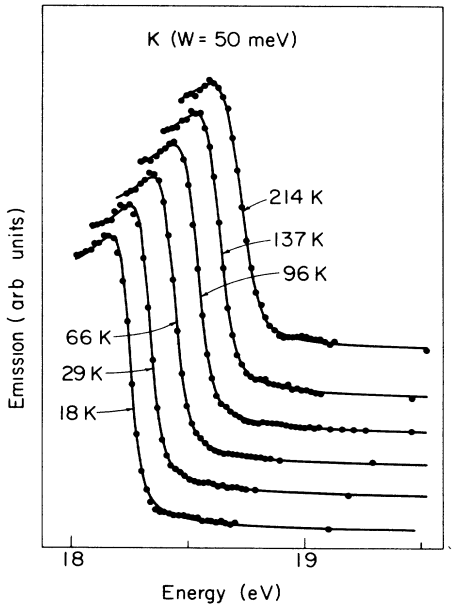

FIG. 18. Fit of edge-shape modeling (lines) for K to data (points) as described in the text. Results for different temperatures are offset for clarity. W is the lifetime Lorentzian width chosen for best fit to all data set. Fits to thicker K films gave $W \sim 17$ meV (see text for discussion).

from Fig. 4, however, that K films of this thickness have an edge width broadened by a surface recombination channel. When data from thicker films are analyzed, we find a much smaller lifetime width that falls in a range $10 \leq \hbar/\tau \leq 24$ meV, which is consistent with an earlier analysis.[30] In our analysis, the surface effect can evidently be subsumed into the model fit reasonably well as a simple increase of the Lorentzian width after spin-orbit subtraction. The general temperature dependencies of the phonon effects deduced for K in Figs. 9 and 15 may well remain reasonably accurate, but an uncritical acceptance of the fitted results can lead to incorrect lifetimes.

With this modification, the deduced core-hole lifetimes are, for Cs, 50±20 meV; for Rb, 25±10 meV; and, for K, 17±7 meV. In earlier work a value for Na of 10 meV was deduced by Callcott, Arakawa, and Ederer[9] from edge shifts believed to arise from incomplete phonon relaxation. The sequence of results reveals for the first time a systematic trend of Auger lifetimes with atomic size through the series of alkali metals. Further matters that bear on the question of the core-hole lifetimes are taken up in Sec. IV C.

C. Emission intensities and higher excited levels

Emission is observed only from the $(n+1)s^2$ levels, and of these the $J=\frac{1}{2}$ hole partner is anomalously weak. This is not the case for the absorption spectra, which extend to high energy with complex structure that resembles the atomic distribution of outer-core oscillator strength. Skinner[2,1] has explained these general characteristics as arising from fast decay processes that short-circuit photon emission from higher levels, to leave observable emission from the lowest excited levels alone. In what follows, the emission results are examined in an effort to understand the dynamics of the decay chains.

The $(n+1)s^2$ excited levels that dominate the emission spectrum of the metal contain only $\sim 10\%$ of the np^6 oscillator strength in the atom (see below). The remainder is mainly divided between higher s and d levels, two-electron excitations, and the continuum.[35,36] Figure 14 shows that in the metal, also, the absorption above threshold rises rapidly through detailed processes that are distinct from the threshold excitation and contain much of the oscillator strength. The features are often less than the plasmon energy (~ 4 eV) in width and therefore correspond to electronically "relaxed" states. In some cases at least, similar excited-state structure is present in the transitional matrix elements from the core orbital to a single band orbital appropriate to the excitation energy.[54] While the atomic spectra of the heavy alkali metals are complicated by abundant two-electron excitations,[36] the strongest low-lying levels are single excitations. These can be mapped onto the solid-state spectra. Figure 14 shows the np^5 spin-orbit splittings identified in this way, and also the $(n+1)snd$ excited valence states. In the Cs atom the d level lies between the s^2 spin-orbit partners, and it appears to be further red-shifted by cohesion in the solid state. In the Rb atom the d level lies above the $J=\frac{1}{2}$ s^2 configuration, but in the metal (Fig. 14) it is red-shifted so that the two cannot be distinguished separately. No explanation has been given for the observed intensities, particularly the weakness of the Cs spin-orbit partner process.

Our purpose is to model the higher excited states in order to reproduce the observed emission from the lowest excited states. The relative emission strengths and widths of the two s^2 levels and sd levels are of immediate interest, as also is a comparison among the total emission yields of the different metals. For the latter, the experimental evidence comprises the relative emission intensities observed from thin-film pairs, as quoted in Sec. III. Figure 19 shows results for the K and Rb spin-orbit partner intensities and widths. The lines through the $J=\frac{1}{2}$ data are $J=\frac{3}{2}$ edges, shifted and reduced appropriately in amplitude, and broadened by an additional Lorentzian width defined in the inset key, then superposed back on the unshifted $J=\frac{3}{2}$ edge profile. The amplitude ratios for the best fit were found to be 47±5 for Rb and 12±1 for K. An excess Lorentzian width of $W'=30\pm10$ meV for K is seen to give reasonable fits to the results in Fig. 19. For Rb, an excess width near 50 meV provides a fair fit (Fig. 19), but the overall shape is not fully satisfactory, apparently because of difficulties with the background slope. A separate fit to the spin-orbit partner alone using an optimal background slope revealed the added edge broadening as about 100 meV. We conclude that the excess width is probably in the range $W'=75\pm30$ meV. This is attributed here to the $J=\frac{1}{2}$ process, even though it coincides with the d level also. No comparable observations of the Cs $J=\frac{1}{2}$ process are available.

We employ a simple model in which all $J=\frac{3}{2}$ hole exci-

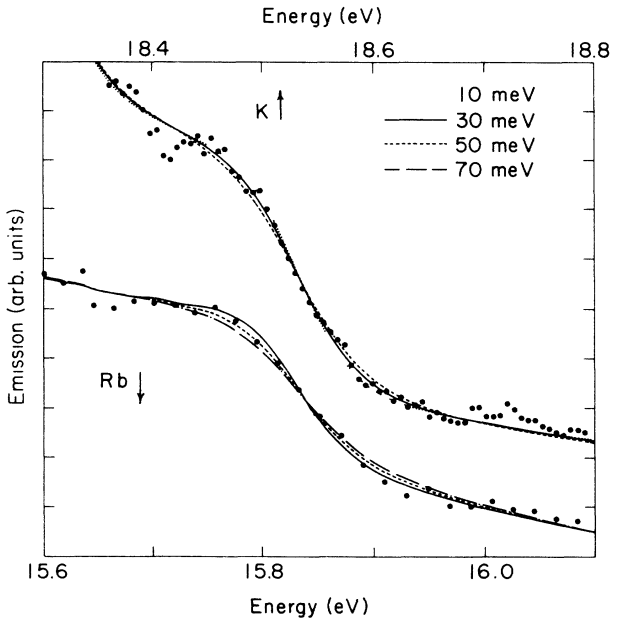

FIG. 19. Excess lifetime broadening for the $P_{1/2}$ spin-orbit partner edges (data points) for K (top) and Rb (bottom). The lines show fits in which the smoothed $P_{3/2}$ band is broadened by Lorentzians of widths indicated in the inset, scaled, shifted, and added to the original band to simulate the $P_{1/2}$ partner.

tations relax to the $(n+1)s^2$, $J=\frac{3}{2}$ configuration and all $J=\frac{1}{2}$ holes relax to the analogous $J=\frac{1}{2}$ state (see Fig. 20). This is consistent with related surface studies that suggest rapid and complete valence relaxation in the core-hole field.[55] In our problem the two levels are presumed to decay by the Auger process with identical rates W that are much faster than the respective photon-emission rates $W_{1/2}$ and $W_{3/2}$. The $J=\frac{3}{2}$ level is fed, in addition, by Coster-Kronig decay[1] from $J=\frac{1}{2}$ with rate W'. For an excitation beam of strength P and total cross sections of $\sigma_{1/2},\sigma_{3/2}$ for the two holes, one finds a ratio of intensities

$$\frac{I_{3/2}}{I_{1/2}}=\frac{1}{\beta}\left[\frac{1}{\alpha}\left[1+\frac{W'}{W}\right]+\frac{W'}{W}\right], \tag{1}$$

and a total intensity $I=I_{3/2}+I_{1/2}$ given by

$$I=\sigma_{3/2}P\left[1+\alpha\left[\frac{W'+\beta W}{W'+W}\right]\right]\frac{W_{3/2}}{W}. \tag{2}$$

In these equations the influence of the relative core-hole–production rates and the optical matrix elements to the s^2 levels are isolated in the ratios $\alpha=\sigma_{1/2}/\sigma_{3/2}$ and $\beta=W_{1/2}/W_{3/2}$. In the first place, Eqs. (1) and (2) will be used to analyze the observations for K and Rb. The possible added effects of the d level will then be mentioned.

With $W=17\pm7$ meV and $W'=30\pm10$ meV for K one must fit the intensity ratio 12 ± 1 using Eq. (1). For the $J=\frac{1}{2}$ and $\frac{3}{2}$ closed shells, $\sigma_{1/2}/\sigma_{3/2}\simeq\frac{1}{2}$. For this value of α, Eq. (1) gives $\beta=0.8\pm0.4$. This result agrees well with the intensity ratio of 2.4 obtained from electron scattering by Slusky *et al.*,[56] which again implies $\beta\sim0.8$. In other research,[57] we have, in addition, observed the lifetime and intensity of the K spin-orbit partners to change consistent with Eq. (1), when the core is placed in other alkali-metal environments, but as if only W is modified. The evidence therefore appears to be in reasonably good accord with the simple modeling. The present detailed fits thus differ somewhat from our earlier tentative conclusions.[6]

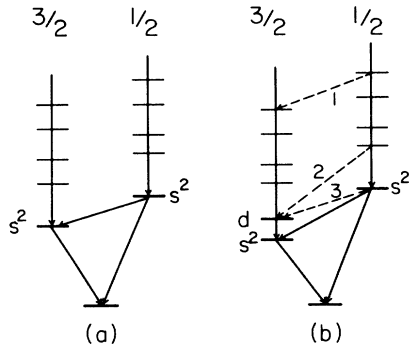

FIG. 20. Sketch of decay chains for $J=\frac{1}{2}$ and $\frac{3}{2}$ holes. (a) The simple model used in the text assumes that each core hole relaxes the metal to the s^2 valence configuration before Coster-Kronig (for $J=\frac{1}{2}$) or Auger decay ($J=\frac{1}{2},\frac{3}{2}$) takes place. More complex processes represented by dashed arrows in (b) could be (1) higher Coster-Kronig transitions including those that (2) avoid or (3) deplete the $J=\frac{1}{2}$ s^2 level through the intervening sd configuration.

For Rb the values $W=25\pm10$ meV and $W'=75\pm30$ meV must fit the intensity ratio 47 ± 5. With $\alpha=\frac{1}{2}$, Eq. (1) gives $\beta=0.35\pm0.2$. This is smaller than the expected value near unity, as if branching ratios from higher levels of a cascade were feeding $J=\frac{3}{2}$ disproportionately (Fig. 20), contrary to the simple model. It is noteworthy, however, that the $J=\frac{1}{2}$ partner for Cs in absorption appears significantly smaller than half the $J=\frac{3}{2}$ edge (Fig. 14). A similar intensity shift for Rb would explain the value of β as arising from reduced matrix elements (i.e., $\alpha<\frac{1}{2}$), but this cannot be confirmed because the $J=\frac{1}{2}$ edge is overlaid by the *nd* process. Such distortions might arise from mixing caused by the near degeneracy with the d level, which is thus identified as a possible cause for the highly anomalous spin-orbit partner intensities of both Rb and Cs. An alternative explanation in which the d levels of Rb and Cs act as conduits for cascades to the $J=\frac{3}{2}$ level that by-pass the $J=\frac{1}{2}$ level [Fig. 20(b)] appears much less plausible. This is the case because in absorption the d resonances appear to be only a factor of ~5 broader than the s^2 processes (Fig. 14). With these lifetimes and oscillator strengths, any large flow through the d levels would produce observable d emission, which, however, is not seen in the actual data.

The Rb data in Fig. 19 differ from those of our earlier report[6] by a modified self-absorption correction. The available data[29,33] for the Rb d resonance in absorption are mutually inconsistent and, unfortunately, this affects the deduced emission spectrum. We have eventually used the reflectance data of Gibbs *et al.*[28] to locate the resonance edges, and have shifted the absorption curves accordingly in the correction procedure. As explained above, the revised $J=\frac{1}{2}$ edge shown in Fig. 19 remains too narrow to fully explain the observed intensity ratio with $\beta=1$. However, it is now consistent with values of β as large as 0.5, which appear reasonable by comparison with α for the Cs absorption spectrum. It is our conclusion that low values of β caused, perhaps, by the intermixing with the nearby d levels, may well be a factor in the highly anomalous spin-orbit partner intensities of Rb and Cs.

The same parameters can be employed in Eq. (2) to compare the observed intensities of emission from the different alkali metals. In addition, these calculations need corrections to account for excitation efficiencies in the electron beam. Also needed are oscillator strengths that fix the relative photon-emission rates $W_{3/2}$ for use in Eq. (1). The relative cross sections were obtained using Bethe's formula (see Sec. II B and the Appendix) in a straightforward way. No experimental oscillator strengths are available, so theoretical values for the atom kindly supplied by McGuire[58] were used, the specific values for the $np^5(n+1)s^2$ combined spin-orbit shells being 0.097 for K, 0.146 for Rb, and 0.141 for Cs. With these parameters, the lifetime widths for K, Rb, and Cs, as obtained from Eq. (2), now follow in the ratios 0.17:0.29:1. These are scaled to give the best fit to other results shown in Table III.

TABLE III. Outer core-hole lifetimes (in meV).

	Li	Na	K	Rb	Cs
Curve fit			15[a]	25[b]	50[b]
			17[b]		
Relaxation shift	16[c]	10[c]	16[b]		
Relative emission			11[b]	19[b]	66[b]
Best value		10	14±4	22±6	58±15

[a]Crisp, Ref. 10.
[b]Present work.
[c]Calcott *et al.*, Ref. 9.

Core-hole lifetimes may also be determined in some cases from the "incomplete relaxation" shift between emission and absorption.[1] For Li and Na Calcott *et al.*[8,9] have estimated lifetimes by a theory of Almbladh[18] using the same monochromator for emission and absorption. Lacking this information, we have nevertheless reconstructed the absorption curve from the thickness dependence of the reabsorption, using methods pioneered by Crisp.[10] The shift so determined for K is 22±10 meV, which leads to a lifetime-width estimate of 16±6 meV. This value is included in Table III also, together with an earlier estimate of 15 meV by Crisp. We believe that the agreement among these different estimates for a given metal may be considerably better than reasonable uncertainties dictate, particularly when the theoretical difficulties involved in an accurate analysis are recognized. Nevertheless, the systematic variation of lifetime with atomic size appears to be established clearly by the results collected in Table II. These deductions therefore warrant future theoretical effort in order that the physical origins of the trends may become better understood. From the experimental viewpoint, it seems likely that synchrotron radiation used as a tunable probe while chosen end products are monitored will become a powerful tool for applications in this area.

V. SUMMARY

In this paper we have described emission characteristics of the heavy alkali metals K, Rb, and Cs. It has been possible to compare these results with earlier data for Na and K to discern systematic changes through the important series of alkali metals from Na to Cs. We find that the different alkali-metal emission bands are remarkably similar when normalized and scaled by their Fermi energies. Each exhibits a strong broadening at the band bottom attributed by Skinner[2] to the lifetime of the band hole of the final state. The bands differ in their "MND anomalies" near E_F, which are generally weaker in emission than in absorption and which dwindle through the series to become undetectable for Cs. The intensity ratio between the $J=\frac{3}{2}$ and $\frac{1}{2}$ spin-orbit partners also varies through the series and greatly exceeds the ideal ratio of 2, reaching ~ 50 for Rb and more for Cs. These arise from Coster-Kronig decay in K and perhaps, in part, for Rb and Cs, also from the dynamics of decay cascades as the energy of higher levels excited by the electron beam is dissipated. Surface-specific emission is observed in films

A detailed study of the metal edge profiles as functions of temperature has been completed. The several sources of broadening include thermal blurring of the Fermi-edge, core-hole, and band-hole lifetime widths, phonon broadening, and the equipment resolution. For K, Rb, and Cs it has been possible to fit the profiles by a constrained model with temperature-independent lifetimes and phonon widths consistent with the theory. The results reveal core-hole lifetime widths that increase systematically from the earlier reported value of 10 meV for Na to 58 meV for Cs. These values are consistent with measurements of relative emission intensity in thin films couples and, for K, with the shift of emission relative to absorption. Thus the dependence of Auger rate on atomic size through the series is, for the first time, revealed. The phonon-creation processes accompanying emission turn out to be in generally reasonable agreement with earlier theoretical predictions. Partial relaxation phenomena appear to play only a small role in Rb and Cs.

Note added. Dr. Charles W. Clark of the National Bureau of Standards has drawn our attention to a paper by D. Petrini [J. Phys. B **14**, L617 (1980)] in which the Auger lifetime of the *atomic* $2p^5 3s^2$ level is calculated to be 0.8 meV, in good agreement with an earlier result of C. E. Theodosiou [Phys. Rev. A **16**, 2232 (1976)]. When Coulomb-induced correlations are included in the wave function using a configuration interaction, the decay rate is increased by a factor of 5 to give a total width of 4 meV. The active ingredient is an admixture of $2p^5 3p^2$ which, Dr. Clark points out to us, couples by a *monopole* operator to the $2p^6 kp$ Auger-decay state; this may explain the striking effect on the atomic lifetime, as described by Petrini.

In regard to the solid-state effects of concern here, we have explained elsewhere[47] how the alkali-metal $(n+1)s^2$ excited orbitals are bound below the conduction-band bottom in the metal, and are therefore not greatly perturbed. The alkali-metal Auger rates in the metal, as detailed above, vary from a factor of 12 for Na metal to almost 2 orders of magnitude faster for Cs metal than the rate for the uncorrelated Na atom as confirmed by Petrini. It is exceedingly improbable that any such large factor could arise from electronic structure within a single-particle model. We infer that core lifetimes in the alkali metals, and their differences from Auger lifetimes of the atom, are probably dominated by the valence-

electron correlations of the local $np^5(n+1)s^2$-like configuration.

If true, this is a significant discovery. For metallic systems it means that descriptions of these local processes that employ basically determinantal wave functions, with the single-particle orbitals perhaps renormalized to quasiparticle states, must eventually be replaced by descriptions that include explicitly correlated wave functions in the calculation of the matrix elements. Elsewhere, we note analogous difficulties for zinc and halogen excitations that exhibit clear Fano resonances in the solid, and for rare-gas centers on metal surfaces and in the bulk.[59] Thus, in the light of Petrini's work, the present results add an important quantitative difficulty to the accumulating evidence that local electronic correlations play a critical role in the matrix elements of core processes in metals.

ACKNOWLEDGMENTS

The assistance and advice of J. E. Cunningham, A. Matheny, and C. Gutleben is gratefully acknowledged. In addition, we thank C.-O. Almbladh, G. D. Mann, S. E. Schatterly, E. J. McGuire, and T. McMullen for helpful communications. This research was supported in part by the U. S. National Science Foundation under Grant No. DMR-86-01593; use was made of University of Illinois Materials Research Laboratory facilities supported by Grant No. DMR-86-12860.

APPENDIX: SELF-ABSORPTION

Immediate reabsorption of emitted radiation within the sample can play a significant role in determining the observed emission line shape at the Fermi edge and at higher energies. Absorption coefficients of the alkali metals due to valence excitations vary smoothly with energy over the width of their emission bands until the onset of the core transitions at E_F. The absorption edge normally overlaps the emission edge and causes an exponential suppression of emission intensity with increasing depth in the sample. Attenuation is much greater on the high-energy side of the Fermi edge. A high-energy cutoff caused by reabsorption can make the edge appear narrower than the true emission spectrum.

For most of the Fermi-edge spectra obtained in this study, the samples were thin enough that self-absorption was not a major factor in the edge shape. In order to examine thick samples (which give large signals), and to make the necessary minor corrections to the edge profiles, we have nevertheless devised rather straightforward procedures to correct for self-absorption.

Crisp[10] and others[60] correct self-absorption effects in electron-stimulated emission by methods which require no independent absorption measurements, but which instead rely on the ability to change the electron-penetration depth by varying the beam energy. To obtain fine focusing, our apparatus sacrifices the flexibility required to adjust the electron-beam energy over a wide range, which makes these methods impractical. Instead, we have used measured absorption coefficients and an empirical ionization efficiency to determine energy-dependent correction factors for each sample thickness. The detailed procedure is outlined in what follows.

An energetic electron in a metal creates core excitations with an efficiency that depends on the electron energy. This energy and hence the excitations efficiency is, in turn, a function of the penetration depth within the solid. The functional forms of the electron-energy loss and ionization efficiency have been the subject of several studies, most recently in the context of quantitative x-ray fluorescence found for chemical analysis. For SXE spectra, Crisp[10] has had good success using an empirical ionization efficiency based on formulas developed for fluorescence at higher energy.[40,61] We have chosen the same function, $\phi(Z)$, with a straightforward modification for off-normal electron incidence and with α, β, and γ known functions that depend on the excitation characteristics (see Ref. 61):

$$\phi(Z)=[\gamma-(\gamma-\phi_0)e^{-\beta\rho Z/\cos\theta_0}](e^{-(\alpha\rho Z/\cos\theta_0)^2}) .$$

Here, θ_0 is the angle of incidence for the incoming electron beam, ρ is the density, and Z is the depth below the sample surface.

The relative attenuation at a given energy is calculated by integrating the excitation efficiency over the penetration depth, and weighting the contribution at each depth by an exponential attenuation factor that depends on the absorption coefficient and the angle of observation. An integral is then performed over the solid angle of light collection. In short,

$$A(\mu,\tau)=\int_0^{\tau}\int_{(\cos\theta)_{\min}}^{(\cos\theta)_{\max}}\phi(Z)e^{-\mu Z/\cos\theta}dZ\,d(\cos\theta) ,$$

with τ the sample thickness, θ the angle of observation, and $\mu=\mu(\hbar\omega)$ the absorption coefficient. The quantity $A^{-1}(\hbar\omega,\tau)$ was then used as a multiplicative correction to the spectrum of interest. In practice, to avoid excessive processing time, the function $A(\hbar\omega,\tau)$ was tabulated for each alkali metal and used with interpolations for the actual correction of spectra.[62]

Some additional points may be mentioned here. Owing largely to spectrometer differences, absorption and emission edges are not, in general, correctly aligned in energy. Therefore, on the assumption of negligible relaxation shift, we have positioned the two spectra relative to one another such that *after* correction for reabsorption the emission and absorption edges cross at their midpoints. An independent method for determining the absorption-edge position using division of a thin sample spectrum by that from a thick sample (akin to changing the electron-beam energy, though subject to background effects) has been used for potassium, where a substantial signal level due to the spin-orbit partner band remains at energies above the absorption edge. These results agree with the alternative alignment method, and confirm that the actual edge shift is 22 ± 10 meV. The K absorption edge as derived in this way is compared with the directly observed spectrum of Ishii *et al.*[33] in Fig. 21. The main features are clearly visible, but the deduced spectrum is

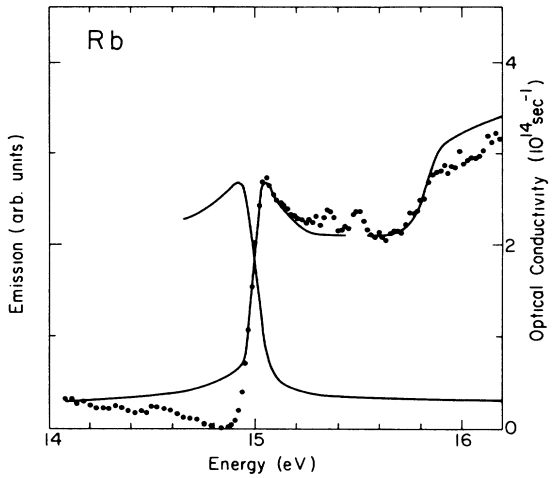

FIG. 21. Optical conductivity of K (solid circles) obtained from comparisons of K emission spectra at various thicknesses as described in the text. This spectrum was used to align published absorption data (Ref. 33) (line) relative to the emission data (open circles). Absolute values for both absorption spectra follow from the scale on the right. The shift between the absorption and emission threshold measured at 70% peak height is 22 meV with a range from about 20 to 40 meV.

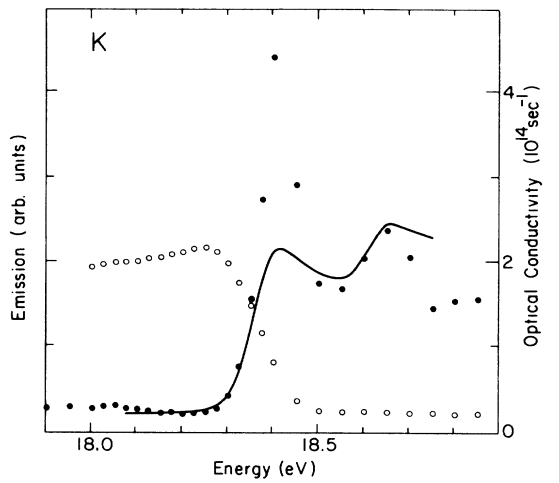

FIG. 22. Optical conductivity of Rb (solid circles) obtained from Rb emission spectrum as in Fig. 21. The line through circles is the published Rb absorption (Ref. 33) and the line crossing it is the Rb spectrum recorded with the CCD array detector. The shift between the absorption and emission thresholds measured at 70% peak height is 15±15 meV.

badly distorted. A similar, more successful, calculation for Rb is illustrated in Fig. 22.

Note that no account is taken of absorption by the sample of radiation from the underlying substrate. For most of our experiments the substrate contribution was kept relatively small by using Li, a poor electron scatterer, as the underlayer. In any case, for thicknesses at which reabsorption becomes most significant the 2-keV electron beam is mainly attenuated by the sample. Neglect of the substrate contribution and refraction effects at the surface of the metal may be justified by the results, as demonstrated by Figs. 4 and 5.

*Present address: Department of Physics, University of Texas, Austin, TX 78712.

†Present address: National Bureau of Standards, Gaithersburg, Md 20899.

[1]For a recent review covering most aspects of the field, see C.-O. Almbladh and L. Hedin, in *Handbook of Synchrotron Radiation* edited by E. E. Koch (North-Holland, Amsterdam, 1983); early viewpoints are reflected in E. H. Burhop, *The Auger Effect* (Cambridge University Press, Cambridge, 1952).

[2]H. W. B. Skinner, Philos. Trans R. Soc. London, Ser. A **239**, 95 (1940).

[3]P. R. Norris, Phys. Lett. **45A**, 387 (1973).

[4]R. H. Kingston, Phys. Rev. **84**, 944 (1951).

[5]P. Fisher, R. S. Crisp, and S. E. Williams, Opt. Acta **5**, 31 (1958); R. S. Crisp, Philos. Mag. **5**, 1161 (1960).

[6]A preliminary report has been published: P. N. First, R. L. Fink, and C. P. Flynn, J. Phys. F **17**, L29 (1987).

[7]T. Kobayasi and A. Morita, J. Phys. Soc. Jpn. **28**, 457 (1970); A. Morita and M. Watabe, *ibid.* **25**, 1060 (1968).

[8]T. A. Callcott, E. T. Arakawa, and D. L. Ederer, Phys. Rev. B **16**, 5185 (1977).

[9]T. A. Calcott, E. T. Arakawa, and D. L. Ederer, Phys. Rev. B **18**, 6622 (1978).

[10]R. S. Crisp, J. Phys. F **10**, 511 (1980).

[11]A. J. Glick and A. L. Hagen, Phys. Rev. B **15**, 1950 (1977).

[12]S. M. Bose, Phys. Rev. B **19**, 3317 (1979).

[13]C.-O. Almbladh, in *X-Ray and Inner-Shell Processes in Atoms, Molecules and Solids,* Conf. Proc. No. X-84, edited by A. Meisel and J. Finster (Technische Hochschule, Ilmenau, 1984), p. 536.

[14]J. J. Ritsko, S. E. Schnatterly, and P. C. Gibbons, Phys. Rev. B **10**, 5017 (1974); P. H. Citrin, G. K. Wertheim, and Y. Baer, *ibid.* **16**, 4256 (1977); T. A. Callcott, E. T. Arakawa, and D. L. Ederer, *ibid.* **16**, 5185 (1977).

[15]C. Kunz, H. Petersen, and D. W. Lynch, Phys. Rev. Lett. **33**, 1556 (1974).

[16]C. P. Flynn, Phys. Rev. Lett. **37**, 1445 (1976).

[17]L. Hedin and A. Rosengren, J. Phys. F **7**, 1339 (1977).

[18]C.-O. Almbladh and A. L. Morales, J. Phys. F **15**, 991 (1985).

[19]T. McMullen and B. Bergersen, Can. J. Phys. **50**, 1002 (1972).

[20]G. D. Mahan, Phys. Rev. B **15**, 4587 (1977).

[21]C.-O. Almbladh, Phys. Rev. B **16**, 4343 (1977).

[22]J. Friedel, Philos. Mag. **43**, 1115 (1952).

[23]J. W. Wilkins, in *X-Ray and Atomic Inner-Shell Physics,* AIP Conf. Proc. No. 94, edited by B. Crasemann (AIP, New York, 1982), p. 687.

[24]C. Swarts, J. D. Dow, and C. P. Flynn, Phys. Rev. Lett. **43**, 158 (1979).

[25]G. D. Mahan, Phys. Rev. **163**, 612 (1967); P. Nozières and C. T. De Dominicis, *ibid.* **178**, 1097 (1969).

[26]H. Neddermeyer, Phys. Rev. B **13**, 2411 (1976). See P. H. Citrin, G. K. Wertheim, and M. Schlüter [*ibid.* **20**, 3067 (1979)] for a detailed treatment of Li, Na, Mg, and Al core absorption and emission edges.

[27]W. J. Carr, Jr., Phys. Rev. **122**, 1437 (1961). For a more recent review of metal-insulator transitions in alkali metals, see A. Ferraz, N. H. March, and F. Flores [J. Phys. Chem. Solids **45**, 627 (1984)] and B. I. Min, T. Oguchi, H. J. F. Jansen, and A. J. Freeman [Phys. Rev. B **33**, 324 (1986)].

[28]Doon Gibbs, T.-H. Chiu, J. E. Cunningham, and C. P. Flynn, Phys. Rev. B **32**, 602 (1985).

[29]S. Sato, T. Miyahara, T. Hanyu, S. Yamaguchi, and T. Ishii, J. Phys. Soc. Jpn. **47**, 836 (1979).

[30]R. S. Crisp, J. Phys. F **13**, 1325 (1983).

[31]E. Jensen (private communication).

[32]C. E. Moore, *Atomic Energy Levels,* Natl. Bur. Stand. Ref. Data. Sys.–Natl. Bur. Stand. (U.S.) Circ. No. 35 (U. S. GPO, Washington, D.C., 1971); M. W. D. Mansfield, Proc. R. Soc. London, Ser. A **346**, 539 (1975).

[33]T. Ishii, Y. Sakisaka, S. Yamaguchi, T. Hanyu, and H. Ishii, J. Phys. Soc. Jpn. **42**, 876 (1977); T. Miyahara, S. Sato, T. Hanyu, A. Kakizaki, S. Yamaguchi, and T. Ishii, *ibid.* **49**, 194 (1980).

[34]S. E. G. Slusky, S. E. Schnatterly, and P. C. Gibbons, Phys. Rev. B **20**, 379 (1979).

[35]M. W. D. Mansfield, Proc. R. Soc. London, Ser. A **364**, 135 (1978).

[36]J. P. Connerade, M. W. D. Mansfield, G. H. Newsom, D. H. Tracy, M. A. Baig, and K. Thimm, Philos. Trans. R. Soc. London, Ser. A **290**, 327 (1979); P. Mitchell, J. Phys. B **12**, 1653 (1979).

[37]J. A. Tagle, E. T. Arakawa, and T. A. Callcott, Phys. Rev. B **21**, 4552 (1980).

[38]M. S. Anderson and C. A. Swenson, Phys. Rev. B **31**, 668 (1985).

[39]M. S. Anderson and C. A. Swenson, Phys. Rev. B **28**, 5395 (1983).

[40]See, e.g., C. J. Powell, Rev. Mod. Phys. **48**, 33 (1976).

[41]R. S. Crisp and S. E. Williams, Philos. Mag. **6**, 365 (1961).

[42]T. McMullen, J. Phys. C **3**, 2178 (1970).

[43]R. P. Gupta and A. J. Freeman, Phys. Lett. **59A**, 223 (1976).

[44]L. Hedin, Phys. Rev. **139**, A796 (1965).

[45]E. Jensen and E. W. Plummer, Phys. Rev. Lett. **55**, 1912 (1985).

[46]J. E. Northrup, M. S. Hybertson, and S. G. Louie, Phys. Rev. Lett. **59**, 819 (1987).

[47]See, e.g., C. P. Flynn [J. Phys. F **10**, L315 (1980)] for solid-state applications; Burhop (Ref. 1) gives references to earlier applications to atoms. For specific applications to the alkali metals, see T-H. Chiu, D. Gibbs, J. E. Cunningham, and C. P. Flynn, Phys. Rev. B **32**, 588 (1985).

[48]R. Haensel, G. Keitel, P. Schreiber, B. Sonntag and C. Kunz, Phys. Rev. Lett. **23**, 528 (1969).

[49]A. Rosengren and B. Johansson, Phys. Rev. B **22**, 3706 (1980).

[50]R. Kammerer, J. Barth, F. Gerken, C. Kunz, S. A. Flodström, and L. I. Johansson, Phys. Rev. B **26**, 3491 (1982).

[51]W. R. Tyson and W. A. Miller, Surf. Sci. **62**, 267 (1977).

[52]F. A. Zhivopistsev and F. E. Comas, Vest. Mosk. Univ. Fiz. **36**, 20 (1981) [Moscow Univ. Phys. Bull. **36**, 23 (1981)]; K. Ohtaka and Y. Tanabe, Phys. Rev. B **30**, 4235 (1984).

[53]V. Ramamurthy and M. Satishkumar, Physica **111B**, 297 (1981); J. R. D. Copley and B. N. Brockhouse, Can. J. Phys. **51**, 657 (1973); R. A. Cowley, A. D. B. Woods, and G. Dolling, Phys. Rev. B **150**, 487 (1966).

[54]J. J. Ritsko, S. E. Schnatterly, and P. C. Gibbons, Phys. Rev. Lett. **32**, 671 (1974).

[55]C. T. Chen, R. A. DiDio, W. K. Ford, and E. W. Plummer, Phys. Rev. B **32**, 8434 (1985).

[56]S. E. G. Slusky, S. E. Schnatterly, and P. C. Gibbons [Phys. Rev. B **20**, 379 (1979)] use fits to electron energy loss data on K at $q=0$.

[57]R. L. Fink and C. P. Flynn (unpublished).

[58]E. J. McGuire (private communication).

[59]See, for example, P. N. First, R. L. Fink, and C. P. Flynn, Phys. Rev. Lett. **60**, 952 (1988).

[60]R. Liefield, in *Soft X-Ray Band Spectra,* edited by D. Fabian (Academic, New York, 1968).

[61]J. D. Brown and R. H. Packwood, X-Ray Spectrom. **11**, 187 (1982).

[62]R. H. Packwood and J. D. Brown, X-Ray Spectrom. **10**, 138 (1981).